Eur Biophys J (2010) 39:1483–1491
DOI 10.1007/s00249-010-0606-y

ORIGINAL PAPER

Structural studies on serum albumins under green light irradiation

Sorin Comorosan · Silviu Polosan · Irinel Popescu · Elena Ionescu · Radu Mitrica · Ligia Cristache · Alina Elena State

Received: 5 October 2009 / Revised: 2 April 2010 / Accepted: 20 April 2010 / Published online: 16 May 2010

Abstract This paper presents two new experimental results: the protective effect of green light (GL) on ultraviolet (UV) denaturation of proteins, and the effect of GL on protein macromolecular structures. The protective effect of GL was revealed on two serum albumins, bovine (BSA) and human (HSA), and recorded by electrophoresis, absorption, and circular dichroism spectra. The effect of GL irradiation on protein structure was recorded by using fluorescence spectroscopy and electrophoresis. These new effects were modeled by quantum-chemistry computation using Gaussian 03W, leading to good fit between theoretical and experimental absorption and circular dichroism spectra. A mechanism for these phenomena is suggested, based on a double-photon absorption process. This nonlinear effect may lead to generation of long-lived Rydberg macromolecular systems, capable of long-range interactions. These newly suggested systems, with macroscopic quantum coherence behaviors, may block the UV denaturation processes.

S. Comorosan (✉) · E. Ionescu
National Institute for Advanced Studies in Electrical Engineering, Bucharest, Romania
e-mail: scomo_acadro@yahoo.com

S. Polosan
Department of Optics and Spectroscopy, National Institute of Materials Physics, Bucharest, Romania

I. Popescu
Department of Surgery, University of Medicine and Pharmacy, Bucharest, Romania

R. Mitrica · L. Cristache · A. E. State
Department of Biochemistry and Biophysics, University of Medicine and Pharmacy, Bucharest, Romania

Keywords Green light effects · Protein circular dichroism · Macroscopic quantum effects · Macromolecular Rydberg systems

Introduction

The aim of this paper is to provide deeper understanding of the newly reported effects of visible light on biological systems. Our results reveal a protective effect of green light (GL) on UV denaturation of macromolecules. In order to develop a mechanism for these unexpected GL effects, we designed a comprehensive study using state-of-the-art technologies.

The interaction of electromagnetic fields with biological structures is well studied. Nevertheless, the large majority of these studies have been concerned with linear effects, within the canonic UV–Vis resonant theory. Our studies reveal nonlinear effects of electromagnetic GL, in experimental setups of multiphoton absorption. This type of effect has been reported since the 1970s (Fröhlich 1970; Comorosan 1970, 1972, 1974, 1976). Basically, the main evidence suggests kinetic and structural modifications of systems under GL irradiation. An antioxidant effect of GL on cellular cultures and nucleic acids was recently recorded (Comorosan et al. 2009). Following these results, we extended our investigations on protein structures. In this paper we examine two serum albumins, bovine (BSA) and human (HSA), using UV denaturation, electrophoresis, circular dichroism, absorption, and fluorescence spectroscopy.

Materials and methods

BSA was purchased from Aldrich Chemicals (Deisenhofen, Germany). HSA was obtained from human blood, screened

for normal chemical parameters, collected in Vacutainer tubes, and centrifuged at 3,000 × g for 15 min. The supernatant serum was removed and used in the experiments. NaCl was obtained from Aldrich Chemicals (Deisenhofen, Germany). Ponceau S dye was obtained from Cellogel Malta (Italy).

UV irradiation was performed using a Vilbert-Lourmat UV lamp, model VL-204 G, 16 W, emitting 90% of the energy at $\lambda = 254$ nm. A special geometry of the setup with irradiation time controlled by an electronic shutter was designed for each experiment to deliver flux of 10.00 J m^{-2} s^{-1}.

For GL irradiation, four powerful light-emitting diodes (LEDs) of 100 lumens each, mounted on ventilated copper radiators, were used. In these setups, designed for each particular type of experiment, monochromatic light of $\lambda = 514$ nm was obtained, with intensity of 3 × 10^5 to 4 × 10^5 lx, as measured by a digital Luxmeter LX-1102, Lutron (4 × 10 to 4 × 10^5 lx range).

UV–Vis spectroscopy was performed by Jasco J815 spectrophotometer. Measurements were made on Hellma Suprasyl quartz cuvette with 1 cm path.

Fluorescence spectra were recorded on Edinburgh Instruments F900 at 90° angle. Measurements were made on Hellma Suprasyl quartz cuvette with 1 cm path.

Circular dichroism measurements were performed on Jasco J815 model using a water-cooled thermostated Peltier device with 0.1°C accuracy, 163–900 nm range, on Hellma Suprasyl quartz cuvette with 0.1 cm path.

For HSA electrophoresis, a complete DiaforEZ—DIAMEDIX Diagnostica line was used.

BSA gel electrophoresis was performed on Alert polymerase chain reaction (PCR) 4% agarose reagent, with precast wells, supplied by Nanogen Advanced Diagnostics (Italy), in Tris–borate–ethylenediamine tetraacetic acid (EDTA)–Na_2 (TBE) buffer. A volume of 4 μL 2% BSA in double-distilled water was mixed with 1 μL Ponceau S dye for each well and run at 12 V cm^{-1} gel length. After migration the samples were removed from the tank, photographed, and stored in the computer.

For density functional theory (DFT) calculations, Gaussian 0.3W software was used.

The irradiation setups used were: (1) BSA; (2) BSA, irradiated with GL for 2 h; (3) BSA denatured by UV for 15 min; and (4) BSA previously irradiated with GL for 2 h, then denatured by UV for 15 min with simultaneous protection by GL irradiation.

Irradiation was performed on 100 μL BSA solution in a transparent polystyrene well with flat bottom, from a 24-well tissue culture plate (Becton–Dickinson Labware, USA). GL irradiation, 4 × 10^5 lx, was performed in air, up-bottom at 1 cm distance, for 2 h.

UV irradiation was performed for 15 min in air, perpendicular, up-bottom at 7 cm distance. For simultaneous irradiation (GL + UV), GL exposure was performed bottom-up, in air, at 1 cm distance for 15 min, and UV irradiation was performed up-bottom, in air, at 7 cm. A volume of 4 μL BSA solution was used for electrophoretic migration.

For HSA electrophoresis, five microspots of 20 μL each from the supernatant serum were placed on a thin glass plate and irradiated. UV denaturation was performed in air, perpendicular, up-bottom at 7 cm distance, for 15 min. Experiments were performed on 20 serum samples selected from our clinical department with normal biochemical parameters. The results and corresponding statistical analysis are presented in Fig. 5a, b, and c, and the standard deviation (SD) in Table 2.

The protective experiment was performed as follows: the serum sample was prepared by previous GL irradiation for 30 min at 4 × 10^5 lx in air, perpendicular, bottom-up, at 1 cm distance, followed by simultaneous UV irradiation, in air, up-bottom, at 7 cm distance, for 15 min. A volume of 20 μL from the samples was extracted by using special cellogel micro-applicator 8P2 and placed on cellogel film, fixed with the cellogel tank bridges, and run for 25 min at 200 V. Finally, samples were colored with Ponceau S and discolored three times for 10 min with acetone. Probes were then stored, and processed using the software.

For spectroscopic determinations, the BSA solutions were prepared as follows: 50 mg NaCl and 10 mg BSA were diluted in 100 mL bidistilled water. Volumes of 3 mL were placed on Petri dishes ($\Phi = 3$ cm) and GL-irradiated at 4 × 10^5 lx, in air, up-bottom, at 1 cm distance, for 30 min.

For the GL + UV protective experiments, GL irradiation was performed up-bottom, in air, at 1 cm distance, for 30 min. Subsequently the GL was placed bottom-up and simultaneous UV irradiation was performed up-bottom for 15 min, in air, at 5 cm distance. Uncertainties in the absorption, fluorescence, and circular dichroism spectra were computed by using the software of the instrument for ten spectra measured on the respective sample.

Results

Figure 1 presents a macromolecular view of the BSA molecule (Lejon et al. 2008). One may see at the boundary levels the polypeptide bonds, the main component of the secondary structure, which influences the molecular symmetry, inducing the chirality of the macromolecule. The inset presents the peptide structure responsible for the far-ultraviolet transitions. The circular dichroism, connected with the $n \rightarrow \pi^*$ transition located at 220 nm and the

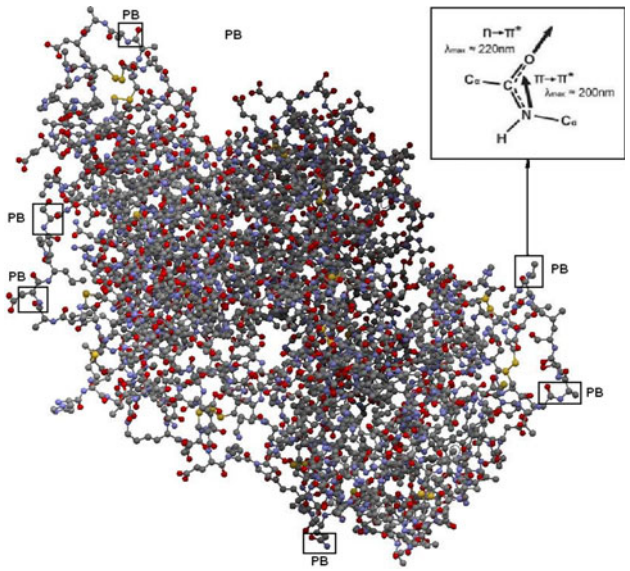

Fig. 1 One may see on the protein structure, at the boundary levels, polypeptide bonds linked to the macromolecule, the main element of our theoretical model. The *inset* shows the orientation of the transition dipoles (*thick arrows*) in the $n \rightarrow \pi^*$ ($\lambda_{max} = 220$ nm) and $\pi \rightarrow \pi^*$ ($\lambda_{max} = 200$ nm) transitions. After Lejon et al. 2008

$\pi \rightarrow \pi^*$ transition located at 209 nm of the peptide group, influences the polypeptide geometry.

Figure 2a presents BSA absorption spectra recorded between 240 and 400 nm. The control recording corresponds to unirradiated BSA solution. The ultraviolet recording represents the sample irradiated for 10 min. The GL + UV recording represents the UV-irradiated sample protected by GL irradiation. As seen from the figure, UV irradiation induces clear denaturation of the BSA molecule, resulting in increase of the 280 nm absorption peak. From the same figure it is clear that GL protection reduces this denaturation effect. A new band located at 315 nm appears as a consequence of UV irradiation, suggesting denaturation of the BSA molecule, an effect also protected by the GL. Concerning the 315 nm band, the excitation and emission spectra show this band in the same position, supporting a scattering effect. The enhancement of this band under UV irradiation and GL protection may suggest clustering of the scattered particles under UV and reduction of this effect under GL.

Figure 2b presents the circular dichroism recording of the BSA molecule. Denaturation of the protein molecules by UV irradiation is recorded. The CD signal at 209 nm is reduced from −175 to −128 mdeg for the UV-irradiated samples. Clear protection due to GL irradiation reduces the CD signal to −141 mdeg.

BSA's mean residue ellipticity (MRE, deg cm^2 dmol^{-1}) was calculated using the relation

$$\mathrm{MRE} = \frac{\theta}{10rl[\mathrm{SA}]},$$

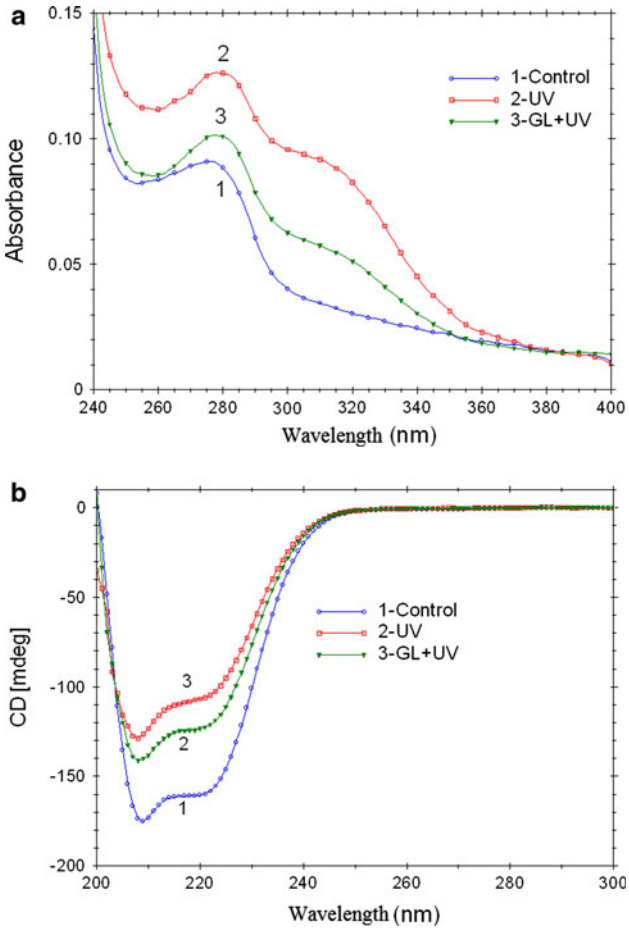

Fig. 2 For UV experiments, samples were irradiated with UV for 10 min. For the protective experiment, samples were irradiated with GL for 30 min followed by simultaneous GL + UV irradiation for 10 min

where θ is the observed CD (in millidegrees), r is the number of amino acid residues (582 for BSA), [SA] is serum albumin concentration, and l is the path length of the cell (in cm). The helical content of BSA for the control, UV, and GL + UV samples was calculated from the mean residue ellipticity determined at 209 nm of CD spectra, using the following equation, as described by Lu et al. (1987):

$$\%\alpha = \frac{\theta_{\mathrm{MRE}} - \theta_0}{\theta_{100} - \theta_0} \times 100,$$

where θ_{MRE} is the mean residue ellipticity for a helix of r amides, compared with the mean residue ellipticity of an infinite helix.

$$\%\alpha - \mathrm{helix} = \frac{-\mathrm{MRE}_{209\mathrm{nm}} - 4,000}{33,000 - 4,000} \times 100.$$

UV irradiation induced denaturation of the BSA molecule, as revealed by the 2.25 ± 0.1% loss of α-helix content (Table 1). When BSA was previously protected

Table 1 Mean residue ellipticity (deg cm^2 $dmol^{-1}$) of BSA, UV-denaturated, and GL-protected samples

Sample	α-Helix (%)
Control	59.08
UV	57.78
GL + UV	58.12

using GL, subsequent UV irradiation produced less protein denaturation, giving 1.65 ± 0.1% loss of α-helix content.

Figure 3a presents the fluorescence emission spectra of control, and UV and UV + GL samples (excited at 280 nm). Under UV irradiation, the fluorescence spectrum of BSA is drastically reduced as a result of denaturation. After GL protection, the fluorescence presents a value intermediate between that of the BSA and the UV-irradiated sample.

Figure 3b presents the fluorescence and excitation spectra of BSA. Both spectra are reduced under GL irradiation, suggesting unfolding of the BSA macromolecules. Since the fluorescence measurements depend on the density of the polypeptides in the measuring area of the instrument, a decrease of the fluorescence intensity is expected to indicate spatial expansion of the respective structures.

Figure 4 presents the BSA gel electrophoresis experiment (Dunn 1997). A clear-cut, significant protective effect may be observed. Under UV irradiation, the BSA molecule appears discolored, fragmented, spread, and less bonded with the Ponceau S dye. In the GL-protected sample, the BSA molecule is clearly less affected by the denaturation process, with the colored spot close to the control frame. The loading for each densitometer scan was rigorously determined for each experiment by micropipetting each volume.

Figure 5 presents the gel electrophoresis recording of an HSA sample. As compared with the control recording, strong denaturation of the albumin fractions under UV is observed, leading to a decrease of the albumin/globulin (A/G) ratio from 1.87 in the control sample to 0.40 in the UV-irradiated one. GL irradiation provided protection, leading to a decrease in A/G ratio of 1.13. The numerical values of these fractions are presented in Table 2.

Figure 6a presents the energy levels of a peptide structure. The contributions of singlet states with oscillator strength higher than 0.1 were used. GL double-photon absorption was added. The presented states may be associated with Rydberg states close to the conduction band. The numbers in the figure were derived from Gaussian software output files which give the singlet energy levels in eV using time-dependent density functional theory (TD-DFT) (Scalmani et al. 2006).

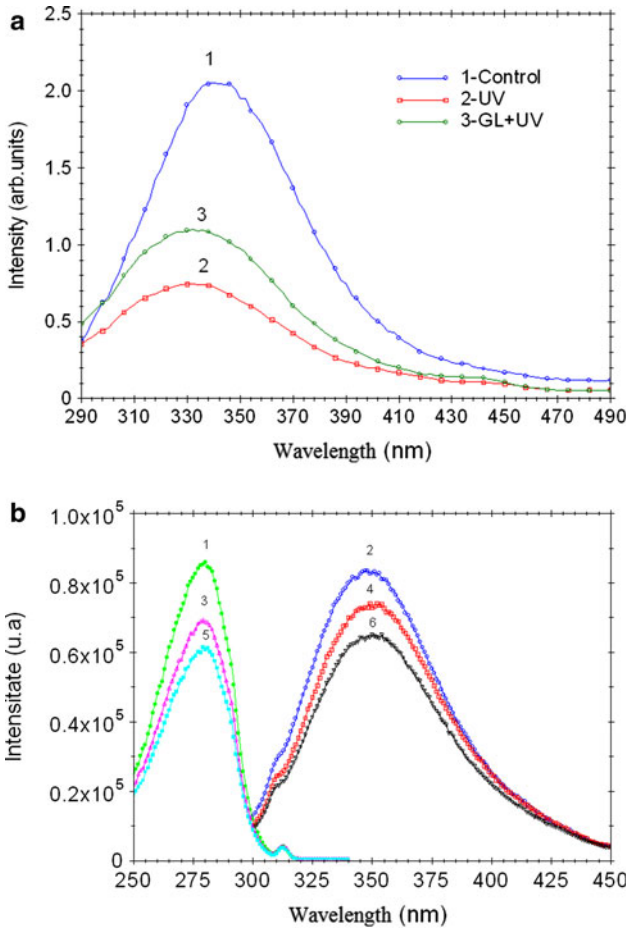

Fig. 3 **a** BSA fluorescence spectra. Control samples (1), probes irradiated with UV for 10 min (2), and probes irradiated with GL for 30 min followed by simultaneous GL + UV irradiation for 10 min (3). **b** BSA fluorescence spectra for the control and GL-irradiated samples. 1-Control, excitation spectrum for emission at 350 nm; 2-control, spectrum for emission excited at 280 nm; 3-GL irradiation for 15 min, excitation spectrum for emission at 350 nm; 4-GL irradiation for 15 min, spectrum for emission excited at 280 nm; 5-GL irradiation for 30 min, excitation spectrum for emission at 350 nm; 6-GL irradiation for 30 min, spectrum for emission excited at 280 nm

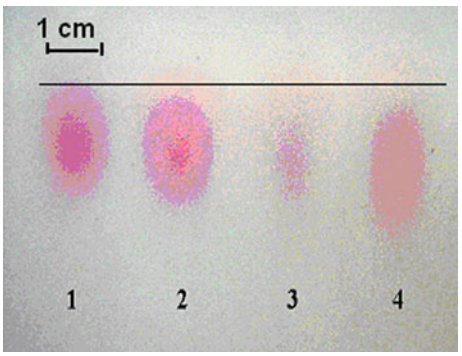

Fig. 4 **1** Control; **2** GL 2 h irradiation; **3** UV 20 min irradiation; **4** GL 2 h and (UV + GL) 20 min irradiation. Electrophoresis was performed on Alert PCR 4% agarose reagent, with precast wells, supplied by Nanogen Advanced Diagnostics (Italy), in TBE (Tris–borate–EDTA–Na_2) buffer

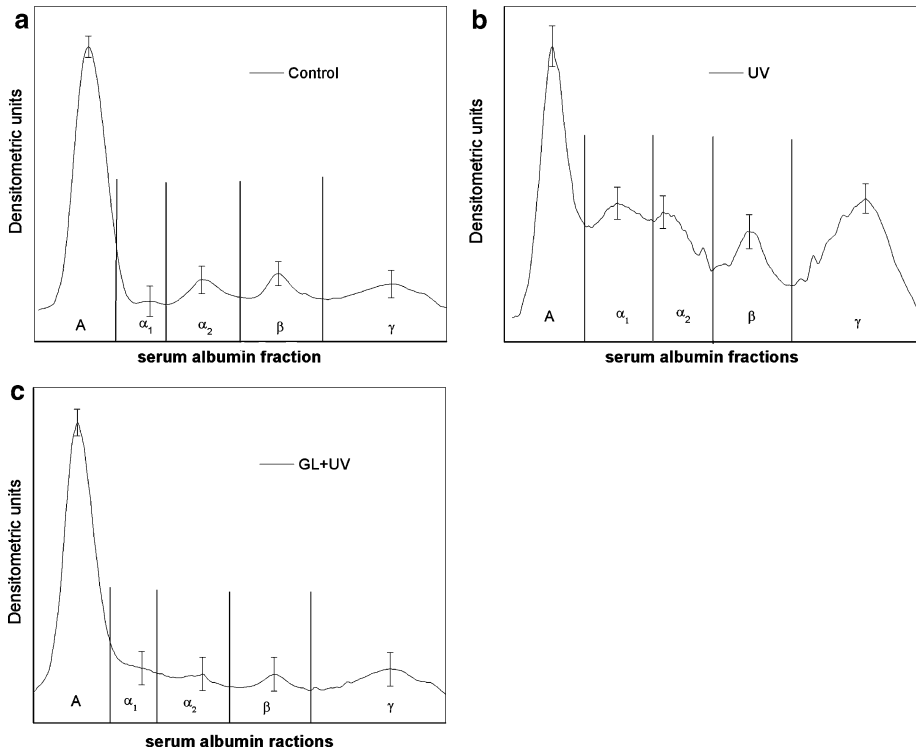

Fig. 5 Recording of the control electrophoresis sample compared with the recordings of UV and UV + GL protected samples

Table 2 Human serum albumin fractions determined by gel electrophoresis

Fractions	Normal values (% of total proteins)	Control (SD)	UV irradiated (SD)	UV + GL irradiated (SD)
Albumin	53.0–65.0	65.2 (±2.55)	28.6 (±1.87)	53.0 (±2.40)
Alpha 1	2.0–5.0	2.2 (±3.65)	15.9 (±1.50)	4.4 (±3.00)
Alpha 2	8.0–14.0	9.9 (±3.28)	14.9 (±1.50)	13.0 (±2.95)
Beta	10.0–15.0	10.1 (±2.92)	14.5 (±1.57)	10.9 (±2.95)
Gamma	11.0–21.0	12.6 (±3.20)	26.1 (±1.35)	18.7 (±3.00)
A/G ratio	1.80	1.87	0.40	1.13

Figure 6b presents a Jablonsky diagram designed to represent the excited levels in the investigated protein (Kasha 1999).

Figure 7a presents the absorption spectrum computed for a peptide structure. Two main absorption bands at 280 and 380 nm can be seen in the experimental spectrum of the BSA solution, well fitted by the computed ones.

Figure 7b presents the electronic circular dichroism computed for the peptide structure, compared with the far-UV CD signal from the BSA solution. The $2n \rightarrow \pi^*$ transition at 228 nm and $\pi \rightarrow \pi^*$ transition located at 202 nm may also be observed in the computed spectrum.

Figure 8a and b presents the highest occupied molecular orbital (HOMO) and lowest unoccupied molecular orbital (LUMO) states of the modeled peptide structures, showing the respective charge distribution. The molecular orbital representations show the behavior of one electron in an electric field generated by the nuclei, together with an average distribution of the other particles.

Discussion

Our experimental results clearly reveal two new phenomena: (1) a protective effect of GL on UV denaturation of proteins, and (2) a structural effect of GL on the protein macromolecular texture.

Both of these aspects are outside the canonical knowledge, which is mainly based on UV–Vis linear resonant theory (Eisenberg and Resnick 1974). Since the described effects reveal nonlinear interactions between GL and biological systems, GL irradiation may induce transitions similar to the Raman and Rydberg phenomenology (Colthup et al. 1990). In our experimental setups,

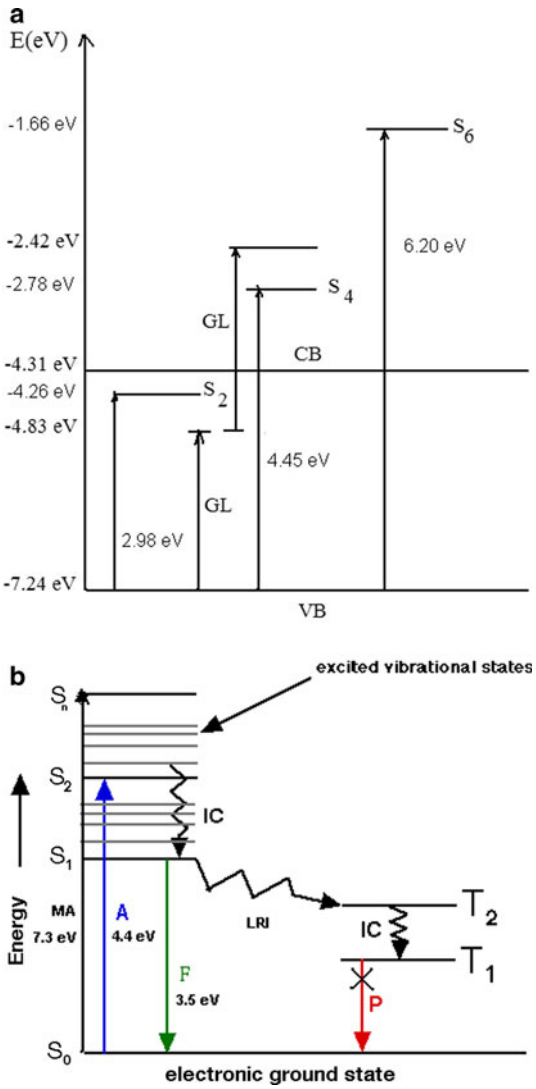

Fig. 6 **a** Energy levels with the main singlet-state transitions S_2, S_4, S_6, and the GL double-photon absorption. VB-valence band, CB-conduction band. **b** Jablonsky diagram representing the excited levels in the investigated protein. A-absorption at 280 nm (4.42 eV), F-fluorescence at 350 nm (3.54 eV), IC-internal conversion, P-phosphorescence, LRI-long-range interaction as suggested by our model

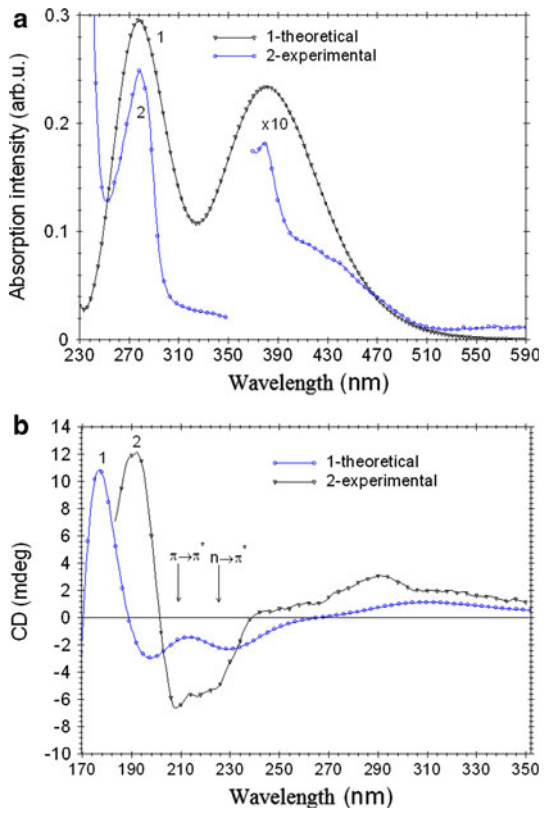

Fig. 7 **a** Calculated oscillator strength spectrum for BSA. The theoretical absorption spectrum was computed for a water solution of peptide, and the experimental absorption spectrum was measured on a water solution of BSA. Absorption in the visible interval between 350 and 590 nm was multiplied by ten in order to highlight the very low intensity of the 380 nm band. **b** The electronic circular dichroism spectrum was computed for a water solution of peptide, and the experimental circular dichroism was determined for a water solution of BSA

GL irradiation may induce alterations of intramolecular forces responsible for maintaining the secondary and tertiary structures, by generating special macromolecular excited states, leading to long-range interactions. These types of effects have been reported long ago (Stevens and Hutton 1960) and are now common in the laser field. When the excited states in such systems are Rydberg states, a Rydberg molecule (or radical) may be created. Rydberg atoms have an electron in a state with high principal quantum number, excited to an energy level that is weakly bound, close to the conduction band, and as a result may favor unusually long-range interactions. This type of effect was revealed in our electrophoresis results.

In the BSA electrophoresis experiment, the GL-irradiated sample appears extended, a feature that may be correlated with the unfolding effect suggested by the fluorescence measurement. This type of effect has been reported by Stan et al. (2009). The same type of electrophoretic effect has also been previously reported on DNA macromolecules (Comorosan et al. 2009).

Our experimental results have been modeled by a quantum-chemical computation which gives the respective highly excited molecular states close to the conduction band (Fig. 6a).

The density functional theory (DFT) (Hohenberg and Khon 1964) calculation was performed on the peptide structure (Fig. 1b) using Gaussian 03W software (Kohn and Sham 1965).

The molecular geometry of the peptide structure was optimized using Kohn-Sharm DFT (Kohn and Sham 1965). The B3LYP hybrid exchange correlation functional (Lee et al. 1988) and the 6-311G* polarized functions were used

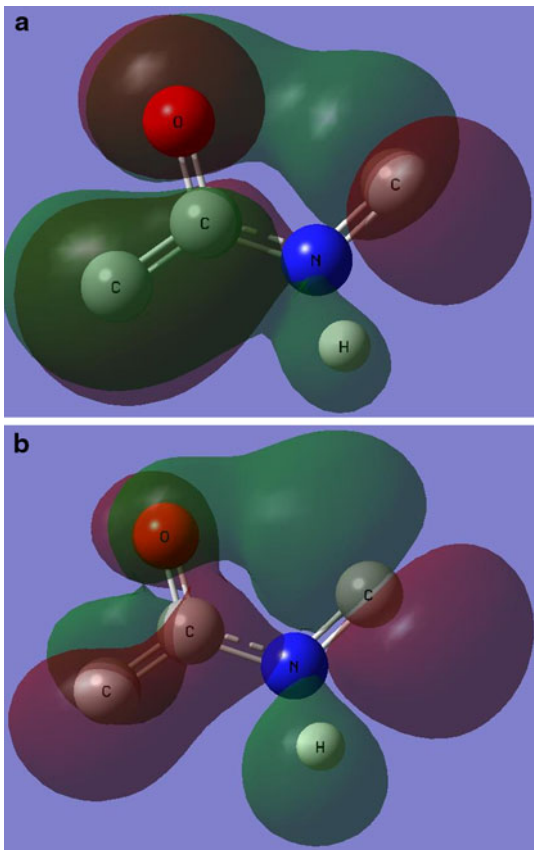

Fig. 8 **a** The charge distribution of a HOMO state for the peptide structure computed using Gaussian View 4.1. *Green* = negative isovalues; *Red* = positive isovalues. One may see from the representation of the orbitals that the negative charge distribution is more extended in the HOMO state as compared with in the LUMO state, which may be correlated with our interpretation of a long-range, long-lived Rydberg-type molecular system. **b** The charge distribution of a LUMO state for the peptide structure computed with Gaussian View 4.1. *Green* = negative isovalues; *Red* = positive isovalues

as basis sets (Raghavachari et al. 1980). This method was used due to the mixing of DFT exchange–correlation and HF exchange. For the basis set, 6-311G* is more suitable for C, O, N, and H atoms, since the charge distribution induces a polarization effect which distorts the shape of the atomic orbitals. The *s* orbitals would display some of the *p* tendency, because of hybridization effects.

The solvation effect was modeled using the polarizable continuum model (PCM) with the integral equation formalism variant (IEFPCM) in water solvent (Tomasi et al. 1999). The PCM method includes an external iteration procedure whereby the program computes the energy in solution by making the solvent reaction field self-consistent with the solute electrostatic potential.

The computed energies are established at a lower level, since in the BSA structure we deal with polypeptides. GL irradiation may generate a series of Rydberg states for the polypeptide structures, which may in turn induce a cooperative effect of quantum macroscopic type, which provides protection against UV denaturation of BSA protein. The denaturation is induced through disulfide bond formation, as described by Ashikava et al. (2000). It is interesting to note that this antioxidant effect was reported through a chemical mechanism, thus emphasizing the novelty of our approach in which the antioxidant effect is induced by GL.

The calculated absorption spectrum is shifted by around 30 nm because of the difference between the peptide unit and polypeptide chains. The blue-shift in the emission spectra (Fig. 3a) is due to the denaturation effect of the UV light, corresponding to conformational changes of the BSA molecule. This is also slightly reflected in the absorption spectra shift (Fig. 2a). This blue-shift may also support our hypothesis of molecular architectural modification. The two main calculated absorption bands are located at 380 and 280 nm. The same bands appear in the experimental absorption of BSA solution. The lowest energy band from 380 nm is associated with a $\pi \rightarrow \pi^*$ transition in the peptide structure, in which a substantial charge density is transferred from oxygen to nitrogen. The higher energy band from 280 nm appears as a result of excitation of higher singlets. The lowest excited singlet with relatively small dipole moment is localized on an individual peptide structure, whereas those with higher energy and large dipole moments show delocalization by charge transfer to the nearest-neighbor peptides of the BSA macromolecule. The same bands in the experimental absorption of BSA solution appear ten times weaker due to a solvation process which takes place between the O and N atoms, similar to quinoline absorption in AlQ_3 (Amati and Lelj 2003).

The calculated electron circular dichroism gives two contributions at 202 nm and 228 nm for the peptide. When the peptide polymerization process takes place, the CD spectrum is constrained at 209 and 222 nm. This peptide effect is well fitted in both theoretically and experiment approaches. The term peptide modeled here is linked to the protein secondary structure of the BSA macromolecule, which creates the molecular asymmetry as presented in the inset to Fig. 1. This is the terminology used in circular dichroism structural studies of proteins (Whitmore and Wallace 2007).

The wavefunctions in the LUMO state (Fig. 8b) are more spatially extended as compared with in the HOMO state (Fig. 8a). As a result, the peptides possess a conjugated system spread over the O, C, and N atoms, consisting of molecular orbitals occupied by delocalized electrons. The energy shift between the theoretical and experimental CD spectra is due the fact that the calculations were performed on a single peptide structure, without taking into account relative interactions with the other peptides in the BSA macromolecules. Beside the water solvation, the

relative interactions between peptide structures and the other amides significantly modify the dielectric constant around the considered peptide structure, inducing contraction of electronic orbitals.

Figure 8a and b supports the idea of atoms in higher excited states, with high quantum number and extended charge density, from the lower to the higher singlet states, thus allowing formation of the weakly bound structures. GL excites the peptide structures into the highest states by the suggested multiphoton absorption process. The highest occupied molecular orbitals (HOMO) have a small spatial charge distribution compared with the lowest unoccupied molecular orbitals (LUMO), even lower than the next LUMO state. Accordingly, since the radial distribution increases, leading to superposition of the molecular orbitals, collectivization of many excited peptide structures may occur, leading to creation of conjugated system(s) and formation of new excited macromolecules. In our interpretation, de-excitation of such a macrosystem would not proceed via fluorescence or phosphorescence, since the effect extends into the nanosecond or even millisecond time scales, up to 15–30 min.

The collective excitation leading to this new effect may be linked to the macroscopic quantum phenomenology, as first introduced into the literature by Penrose (1998) and Leggett (2002).

A Jablonsky diagram (Fig. 6b) emphasizes our suggested mechanism (Kasha 1999). The 280 nm (4.42 eV) excitation, 350 nm (3.54 eV) fluorescence, and multiphoton absorption up to 171 nm (7.23 eV) are presented. The de-excitation processes, such as internal conversion (IC), intersystem crossing (ISC), and phosphorescence from the triplet states, may be only predicted, since such processes are replaced by long-range interactions.

The theoretical absorption and CD spectra, computed using Gaussian software, show good agreement with the experimental ones. The computed absorption bands from 280 and 430 nm, as well as the two negative CD bands at 202 and 229 nm, are well fitted, suggesting that all the investigated spectroscopic properties of BSA macromolecules are given by the peptide structures. The fitting is quite reasonable, even though a series of parameters not included in the Gaussian software are neglected (for example, the spin–orbit coupling for the triplet-state intensities is not included in the software and appears zero; the macromolecular density does not appear since we worked on a single macromolecule; the real solvent of water + NaCl was neglected, and the calculation was performed according to the water solvent given by the software).

According to the discussion above, a mechanism for the GL protective effect may be suggested: UV irradiation with 4.88 eV (254 nm) photons induces denaturation of the molecular structures. Under GL irradiation with 2.41 eV (514 nm) photons of high energy density, a nonlinear multiphoton absorption effect may take place, generating Rydberg molecular systems. These long-lived molecular systems, capable of long-range interaction, may block the UV excitation, previously occupied by the two-photon GL absorption process.

Such a protective effect, particularly as revealed by GL irradiation of HSA (Fig. 5), may have significant implications for the medical field. We briefly stress now the physical consistency of the suggested Rydberg-type GL-induced long-range long-lived macromolecular systems.

All our results suggest long-range interactions. This means that we are dealing with transitions that take place in the microscopic environment. In this context, transitions within a few molecules may induce changes in the structure of all macromolecular systems. Let us finally observe that this type of ultralong-range Rydberg molecular systems now represents an active field of investigation in physics (Greene et al. 2000, Boisseau et al. 2002, Bendkowsky et al. 2009).

References

Amati M, Lelj F (2003) Luminescent Compounds fac- and mer-Aluminum Tris (quinolin-8-olate). A pure and hybrid density functional theory and time-dependent density functional theory investigation of their electronic and spectroscopic properties. J Phys Chem A107:2560–2569

Ashikava T, Motoyama A, Ichikawa H, Itagaki H, Sato Y (2000) Low molecular peptide model of protein denaturation by UVA irradiation and the effect of antioxidants. Altern Anim Test Exp 7(1):30–36

Bendkowsky V, Butscher B, Nipper J, Shaffer J, Löw R, Pfau T (2009) Observation of ultralong-range Rydberg molecules. Nature 458:1005–1008

Boisseau C, Simbotin I, Côté R (2002) Macrodimers: ultralong range Rydberg molecules. Phys Rev Lett 88:133004–133007

Colthup NB, Daly LH, Wiberley SE (1990) Introduction to infrared and Raman spectroscopy, 3rd edn. Academic, London

Comorosan S (1970) The biochemical flip-flop. Nature 227:64–65

Comorosan S (1974) The measurement problem in biology. Int J Quantum Chem Symp 1:221

Comorosan S (1976) Biological observables. In: Rosen R (ed) Progress theoretical biology. Academic, New York, pp 161–203

Comorosan S, Vieru S, Murgoci P (1972) The effect of electromagnetic field on enzymic substrates. Biochim Biophys Acta 268:620–621

Comorosan S et al (2009) The green light effects on biological systems: a new biophysical phenomenology. J Biol Phys 35:265–277

Dunn MJ (1997) Quantitative two-dimensional gel electrophoresis. Biochem Soc Trans 25:248–254

Eisenberg R, Resnick R (1974) Quantum physics, electronic spectra. In: John (ed) Wiley & Sons, New York, pp 467–470

Fröhlich H (1970) Long range coherence and the activity of enzymes. Nature 228:228–234

Greene CH, Dickinson AS, Sadeghpour HR (2000) Creation of polar and nonpolar ultra-long-range Rydberg molecules. Phys Rev Lett 85:2458–2461

Hohenberg P, Khon W (1964) Inomogeneous electron gas. Phys Rev 136:B864–B871

Kasha M (1999) From Jablonski to femtoseconds. Evolution of molecular photophysics. Acta Phys Pol A 95:15–36

Kohn W, Sham LJ (1965) Self-consistent equations including exchange and correlation effects. Phys Rev 140:A1133–1138

Lee C, Yang W, Parr RG (1988) Development of the Colle-Salvetti correlation-energy formula into a functional of the electron density. Phys Rev B37:785–789

Leggett AJ (2002) Testing the limits of quantum mechanics. J Phys Condens Matter 14R:415–451

Lejon S, Cramer JF, Nordberg PA (2008) Structural basis for the binding of naproxen to human serum albumin in the presence of fatty acids and the GA module. Acta Crystallogr, Sect F 64:64–69

Lu ZX, Cui T, Shi QL (1987) Application of circular dichroism (CD) and optical rotatory dispersion (ORD). Molecular biology. Science, Beijing

Penrose R (1998) Quantum computation, entanglement and state reduction. Philosophical transactions of the royal society A: mathematical. Phys Eng Sci 356(1743):1927–1939

Raghavachari K, Binkley JS, Seeger R, Pople JA (1980) Self-consistent molecular orbital methods. 20. Basis set for correlated wave-functions. J Chem Phys 72:650–654

Scalmani G, Frisch MJ, Mennucci B, Tomasi J, Cammi R, Barone V (2006) Geometries and properties of excited states in the gas phase and in solution: theory and application of a time-dependent density functional theory polarizable continuum model. J Chem Phys 124(094107):1–15

Stan D, Matei I, Mihailescu C, Savin M, Matache M, Hillebrand M, Baciu I (2009) Spectroscopic investigantions of the bidding interaction of a new indanedione derivate with human and bovine serum albumins. Molecules 14:1614–1626

Stevens R, Hutton E (1960) Radiative Life-time of the pyrene dimer and the possible role of excited dimers in energy transfer processes. Nature 186:1045–1046

Tomasi J, Mennucci B, Cancès E (1999) The IEF version of the PCM solvation method: an overview of a new method addressed to study molecular solutes at the QM ab initio level. J Mol Struct (Theochem) 464:211–226

Whitmore L, Wallace BA (2007) Protein secondary structure analyses from circular dichroism spectroscopy: methods and reference databases. Biopolymers 89(5):392–400